

RESEARCH ARTICLE

10.1029/2019JC015222

Key Points:

- The phenological metrics such as bloom amplitude and timings of central Ross Sea Polynya bloom were determined by a fitting method
- The bloom amplitude continuously tends to increase due to springtime ice loss related to the changed wind direction
- The recently modified Ekman dynamics might drive the westward spread of the central Ross Sea phytoplankton bloom

Supporting Information:

- Supporting Information S1

Correspondence to:

Y.-H. Jo,
joyoung@pusan.ac.kr

Citation:

Park, J., Kim, J.-H., Kim, H.-c., Hwang, J., Jo, Y.-H., & Lee, S. H. (2019). Environmental forcings on the remotely sensed phytoplankton bloom phenology in the central Ross Sea Polynya. *Journal of Geophysical Research: Oceans*, 124, 5400–5417. <https://doi.org/10.1029/2019JC015222>

Received 15 APR 2019

Accepted 10 JUL 2019

Accepted article online 17 JUL 2019

Published online 1 AUG 2019

Environmental Forcings on the Remotely Sensed Phytoplankton Bloom Phenology in the Central Ross Sea Polynya

Jinku Park¹ , Jeong-Hoon Kim², Hyun-cheol Kim² , Jihyun Hwang¹ ,
Young-Heon Jo¹ , and Sang Heon Lee¹ 

¹Department of Oceanography, Pusan National University, Busan, South Korea, ²Korea Polar Research Institute, Incheon, South Korea

Abstract We investigated the interannual variability of the phytoplankton bloom in the central Ross Sea Polynya derived from the annual phenology metrics of the bloom based on ocean color satellite measurements obtained between 2002 and 2017. The phenology metrics determined by the adjusted Gaussian fitting method include the bloom amplitude (BA), bloom initiation timing (BIT), and bloom peak timing (BPT). We found the following results for three phenology metrics. The BA tended to increase since 2002, probably related to the formation of open water area by the atmospheric circulation changes on the synoptic scale over the Ross Sea. The significant sea ice loss trend due to the changing winds over the entire southern coast of the Ross Sea was found. Continuous winds in widened open water can move surface water masses more easily along the wind direction, transferring water masses or chlorophyll pigments themselves accordingly. This process has led to the recent intense bloom in the central Ross Sea Polynya. The interannual variability of the BIT is a function of the sea surface temperature in November and wind speed in October, implying that there is a strong association between ice drift and melting, which can be primarily related to the onset of the polynya expansion. Although there was no direct factor to the BPT, it was somewhat related to the BIT and BA. In other words, the environmental factors forming the BIT and BA might have indirectly influenced the BPT, suggesting that early polynya and large biomass could lead to promoting the bloom decay.

1. Introduction

The Ross Sea (RS) has the highest phytoplankton productivity in Antarctica, contributing 28% of the total productivity of the Southern Ocean (Arrigo, Weiss, & Smith, 1998; Jones & Smith, 2017), with an average maximum chlorophyll-a concentration (CHL) of $>6 \text{ mg/m}^3$ during the austral summers (Arrigo & van Dijken, 2004; Peloquin & Smith, 2007; Ryan-Keogh et al., 2017; Smith, Dinniman, et al., 2003). Satellite-derived CHL concentration maps produced over the past 15 years (2002–2017) have shown a wide distribution over the entire continental shelf of patches containing high CHL concentrations ($>3 \text{ mg/m}^3$; Figure 1). These CHL blooms are highly correlated with polynya dynamics during the austral spring and summer (Arrigo et al., 2015; Arrigo & van Dijken, 2003; Arrigo & McClain, 1994). The Ross Sea polynya (RSP), which is one of the largest polynyas around Antarctica, extends north from the Ross Ice Shelf (RIS). During early spring, the intensified solar irradiance causes the RSP to start to expand rapidly (Arrigo & van Dijken, 2003; Arrigo et al., 1998; Arrigo & van Dijken, 2004); this expansion is accompanied by a large phytoplankton bloom (Arrigo, Weiss, & Smith, 2015; Arrigo & McClain, 1994).

The seasonal phytoplankton blooms associated with the expansion of the RSP (Arrigo et al., 2008; Arrigo & van Dijken, 2003) start in late October, when there is a reduction in sea ice, an increase in irradiance, and shoaling of the mixed layer depth (Jones & Smith, 2017; Smith et al., 2010). During the austral spring and early summer (November–December), strong offshore winds result in weak stratification (a deep mixed layer depth; Arrigo et al., 2003; Arrigo & van Dijken, 2003; Bromwich et al., 1992; Mangoni et al., 2017), and a large bloom dominated by *Phaeocystis antarctica* (*P. antarctica*) develops (Mosby & Smith, 2017; Smith et al., 2013). The bloom accounts for approximately 95% of the total phytoplankton bloom in the RSP (Mangoni et al., 2017). The abundance of *P. antarctica* rapidly declines in late December and early January (Jones & Smith, 2017; Smith et al., 2014) over a period of days to weeks (Smith et al., 2011), and diatoms become more prevalent in the RSP (Mosby & Smith, 2017; Peloquin & Smith, 2007; Ryan-Keogh et al.,

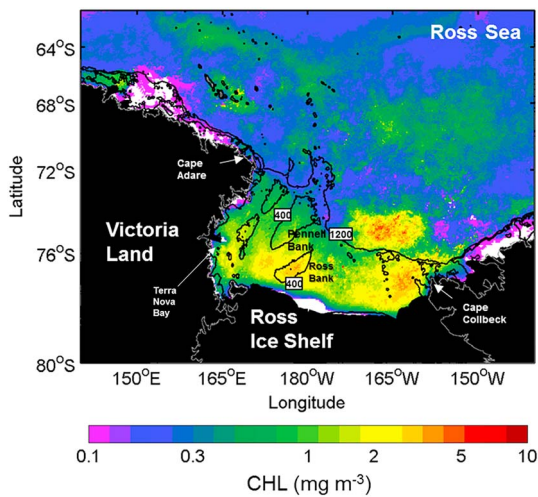


Figure 1. Map of the climatology of chlorophyll-a concentration (log scale) derived from Moderate Resolution Imaging Spectroradiometer during 15 austral springs and summers (2002–2017). Black contour lines indicate the topography 400- and 1,200-m depths.

2017; Smith et al., 2014). This *P. antarctica*-diatom progression of the phytoplankton bloom occurs in response to changes in various environmental conditions (Boyd et al., 2012), but it is primarily a result of the interaction between irradiance and micronutrients such as iron (Boyd, 2002; Jones & Smith, 2017; Peloquin & Smith, 2007; Ryan-Keogh et al., 2017; Sedwick et al., 2011).

Interannual and long-term changes in the seasonality of the phytoplankton biomass can, therefore, have a significant impact on the ecosystem through the disruption of trophic connections (Ji et al., 2010). Moreover, phytoplankton may be useful indicators of climate change (Taylor et al., 2002), contributing to the nonlinearities in the connections between physical forcing and ecosystem productivity (Di Lorenzo & Ohman, 2013; Foukal & Thomas, 2014; Kirby & Beaugrand, 2009). Consequently, knowledge of the modulation of phytoplankton phenology in response to climate-induced changes is essential for understanding the adaptive strategies of phytoplankton in dynamic environments (Boyd et al., 2012). However, little is known about the environmental factors that affect phytoplankton growth and standing stocks or about the variation in phytoplankton blooms that affect the pelagic food web (Mangoni et al., 2017; McGillicuddy et al., 2015).

In general, the timings associated with initiation, peak, and termination and amplitude of the bloom are known to be essential properties for defining the phytoplankton phenology (Ji et al., 2010; Platt et al., 2009; Racault et al., 2012; Salgado-Hernanz et al., 2019). Many studies have attempted to understand the seasonal cycle of the phytoplankton using satellite data using the metrics in the global ocean (Racault et al., 2012; Sapiano et al., 2012), the Northwest Atlantic Ocean (Platt et al., 2009; Platt & Sathyendranath, 2008), the sub-arctic North Pacific Ocean (Sasaoka et al., 2011), the Mediterranean Sea (Salgado-Hernanz et al., 2019), the Scotian Shelf (Zhai et al., 2011), and the East/Japan Sea (Yamada & Ishizaka, 2006). However, most of the studies on interannual variability in the CHL phenology were conducted in the nonpolar regions. Since the polar regions have extensive cloud covers, which obscure the satellite-derived CHL observation, only a few studies on CHL phenology have been carried out in those regions (Marchese et al., 2017; Rubao et al., 2013; Soppa et al., 2016). Moreover, in the RS, the studies on the long-term interannual variability in the CHL phenology are extremely rare or have relied on in situ data.

The present work aims to establish the patterns of variability and trends in the representative CHL phenology of the central RSP bloom by applying the adjusted Gaussian fitting method to the CHL concentrations obtained from satellite observations. The adjusted Gaussian fitting method used was based on that presented by Yamada and Ishizaka (2006). Then, we determined the bloom properties during a growing season from some phenology metrics such as bloom amplitude (BA), bloom initiation timing (BIT), and bloom peak timing (BPT) and investigate the forcings that drive the interannual variability in individual bloom property, focusing in particular on the bloom dominated by *P. antarctica*, which cooccurs with the expansion of the central RSP between October and December.

2. Data Collection

2.1. Data Collection

Satellite-retrieved CHL concentration data from 2002 to 2017 were used to investigate the phenological features and the interannual variability in phytoplankton in the RSP. The CHL pigment data from the Moderate Resolution Imaging Spectroradiometer on Aqua (MODIS-A) are provided by the Ocean Biology Processing Group at the National Aeronautics and Space Administration (NASA; <http://oceancolor.gsfc.nasa.gov>). These data are available at spatial resolutions of 4 and 9 km; the latter was selected for the present study because of the scale of the study area. In terms of temporal resolution, daily, weekly, and monthly composites of the MODIS-A CHL concentration data are available. Although the highest temporal resolution, the daily composite, is most appropriate for obtaining representative phenology, this had frequent coverage gaps due to cloud cover. We, therefore, used the monthly composite to gain an overview of the bloom

characteristics and the weekly composite to analyze the phytoplankton phenology. Of note, the use of ocean color to quantify CHL concentrations has limitations. The accuracy of satellite-derived CHL concentrations in the RS, when compared to in situ measurements, has been estimated as approximately $\pm 65\%$ compared to in situ data (Kaufman et al., 2014; Saba et al., 2011). Arrigo and van Dijken (2004) compared in situ CHL obtained from three cruises during 1997–1998 at 27 stations in the RS and the satellite-derived CHL. Their results showed an average difference in CHL between two data sets of less than 9% (in situ CHL: 2.82 mg/m^3 ; satellite-derived CHL: 3.10 mg/m^3), with a similar standard error (in situ CHL: 3.02 mg/m^3 ; satellite-derived CHL: 2.84 mg/m^3). Although the CHL minimum value differed slightly (in situ CHL: 0.18 mg/m^3 ; satellite-derived CHL: 0.35 mg/m^3), the maximum value showed a close match (in situ CHL: 11.14 mg/m^3 ; satellite-derived CHL: 11.22 mg/m^3). Overall, the two data sets showed a strongly linear relationship, with a correlation coefficient of 0.87. However, these comparisons based on measurements made at a few specific times during the late 1990s, and it is necessary to evaluate the accuracy of satellite observations in this region continuously. The present study investigated the variability of the bloom characteristics associated with the maximum CHL based on the result of Arrigo and van Dijken (2004), so there was unlikely to be an issue with using the satellite-derived CHL data.

The following environmental factors that contribute to the interannual variability in phytoplankton phenology were selected for analysis: the atmospheric temperature at 2 m (AIRT), sea surface temperature (SST), wind speed (Wspd), wind direction (Wdir), sea ice concentration (SIC), and photosynthetically active radiation (PAR). AIRT and SST were both used to determine the effect of temperature on the phytoplankton bloom. The SST data were obtained from the U.S. National Oceanic and Atmospheric Administration daily Optimum Interpolation SST data set, combined with observations from satellites, ships, and buoys (<https://www.ncdc.noaa.gov/oisst>). This data set has a spatial grid resolution of 0.25° and includes data from the Advanced Very High Resolution Radiometer in two versions, with or without data from the Advanced Microwave Scanning Radiometers. The latter was used in this study (Banzon et al., 2016). Unfortunately, in situ and satellite observations tend to be sparse in the RS, particularly in the marginal ice zone. Missing data were generated using proxy estimates of SSTs based on the SIC in the region. The area entirely covered by sea ice has a freezing point of -1.8°C , and the interpolation was conducted along the marginal ice zone (Reynolds et al., 2007). These data were used without any individual data masking to represent the effect of the ice edge when the marginal ice zone was included in the study area. The AIRT, Wspd, and Wdir data were obtained from the National Centers for Environmental Prediction/National Center for Atmospheric Research Reanalysis, launched in 1991 to produce a retroactive record of >50 years of global analyses of atmospheric fields to support the needs of the research and climate monitoring communities (Kalnay et al., 1996; Kistler et al., 2001). The monthly mean data since 1948 are available on the National Oceanic and Atmospheric Administration Earth System Research Laboratory website (<https://www.esrl.noaa.gov/>), at a spatial resolution of 2.5° . The SIC data were derived from the Special Sensor Microwave Imager and the Special Sensor Microwave Imager/Sounder passive microwave radiometer data set, provided by the National Snow and Ice Data Center (<http://nsidc.org/data/nsidc-0051>). This data set comprises daily observations from January 1988 to December 2014 at a 25-km resolution. The SIC was calculated from brightness temperature data using the NASA Team sea ice algorithm developed by NASA's Goddard Space Flight Center and produced by National Snow and Ice Data Center (Cavalieri et al., 1996). Weekly and monthly composites of PAR were obtained from MODIS-A at a spatial resolution of 9 km.

3. Methodology

3.1. Determination of Central RSP Bloom Area

The RS is much more limited to remotely observe the CHL by cloud cover throughout the year (Figure 2). Such observations are only permitted in the austral spring and summer within restricted regions. In general, the CHL concentration distribution could not be determined until October because of the dense clouds and sea ice covers (Figure 2a). The cloud-free regions begin to appear around the continental shelf at the beginning of November (Figure 2b). During November, the shelf, mainly around the Ross Bank (approximately 170°E , 76°S), is characterized by a patch with a high CHL concentration ($\geq 2 \text{ mg/m}^3$). The maximum values of this bloom persist until December (Figure 2c) and then rapidly decline to negligible levels in January (Figure 2d; Jones & Smith, 2017; Smith et al., 2014). Patches with relatively high CHL concentrations also

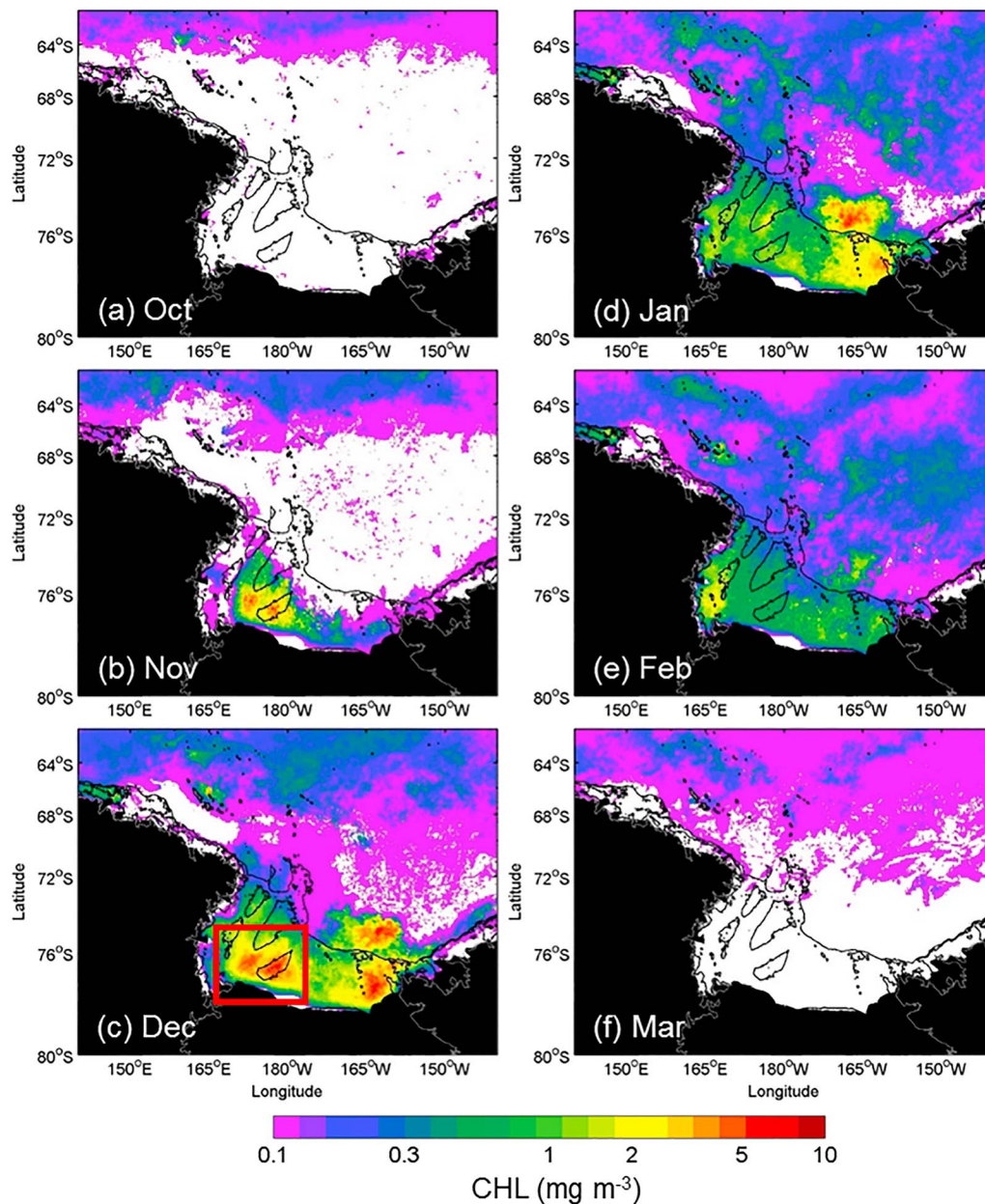


Figure 2. Maps of monthly climatology (2002–2017) of Moderate Resolution Imaging Spectroradiometer chlorophyll (CHL) concentration (log scale) between (a) October and (f) March of the following year. The red box (170°E to 175°W, 75–78°S) in (c) represents the bloom area of central Ross Sea Polynya extracted by k-means clustering. The black contour lines indicate the bathymetry of the Ross Sea with 400-m depth intervals (400–1,600 m). White areas represent missing data due to the cloud and sea ice.

appear in the eastern RS (east of 170°W, between 73°S and 78°S), mainly in the eastern part of the shelf and extending north of the shelf break. Some fractions of these patches to the north of the eastern shelf break remain until February; however, most vanish by this time (Figure 2e). In February, a bloom of $\geq 2\text{-mg/m}^3$ CHL appears in the western RSP around Terra Nova Bay, a region where diatom blooms dominate (comprising approximately 90% of the phytoplankton), due to the relatively shallow mixing layer resulting from the melting of ice in the summer (Arrigo & van Dijken, 2004; Mangoni et al., 2017). The cloud cover begins to increase again in February (Arrigo & van Dijken, 2004). Then, most of the shelf is covered with clouds in March, and satellite observations of the ocean color are no longer possible (Figure 2f).

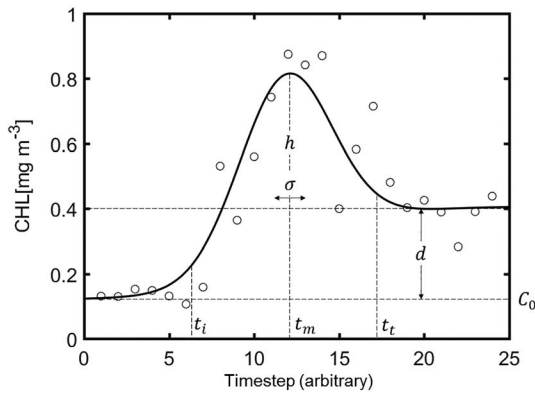


Figure 3. Schematic of the adjusted Gaussian fit model to characterize a phytoplankton bloom. The circles indicate the satellite-retrieved chlorophyll (CHL) concentration data, and the solid black line means a fitted Gaussian curve. h is a bloom amplitude, and d is a residual of CHL concentration. The metrics t_i , t_m , and t_t are bloom initiation time, bloom peak time, and termination, respectively.

By reason of such temporal restriction, the satellite-derived CHL data in the RS are confined only from November to February. In addition, since it is restrictively possible to observe in a specific region, to determine the CHL phenology for each pixel as in the previous study was challenging. Then, in the present study, the CHL concentrations on all available pixels belonging to the bloom area were spatially averaged and used as the primary data for the determination of CHL phenology. Since there is considerable spatial and temporal variability in the standing stocks of the RS phytoplankton during the austral spring and summer (Mangoni et al., 2017; Mosby & Smith, 2017), the determination of bloom area is very difficult. The phytoplankton communities of the central RSP (around the Ross Bank) are dominated alternately by *P. antarctica* and diatoms, with both exhibiting spatial and temporal variability (Arrigo & van Dijken, 2003; Coale et al., 2003; Kaufman et al., 2014; Sedwick et al., 2000; Sedwick & DiTullio, 1997). When the phytoplankton blooms of the two species overlap in time and space, it is quite limited to isolate the bloom by only one species completely. We, therefore, applied k-means clustering to extract the bloom areas in the central RSP for each individual year by in November and December (time the bloom occur;

Figure 2, red box). By this method, it is possible to minimize the influence of the nontarget bloom that may appear in the same space at different times. The location of the final defined bloom area was not constant from year to year because of the spatiotemporal complexity of the central RS phytoplankton bloom (Mangoni et al., 2017). Then, the study area was therefore delineated as a rectangular region including all of the extracted yearly bloom areas; this was visually confirmed to be reasonable concerning the annually recurrent blooms.

3.2. Calculation of Phenology Metrics

In order to extract representative CHL phenology from the satellite-derived data alone, the adjusted Gaussian curve fitting method was used. This method makes it possible to infer CHL dynamics continuously based on the real data that exists a little bit. The adjusted Gaussian-fitted CHL curve, $C(x)$, used in the present analysis, can be expressed by the following equation:

$$C(x) = C_0 + h \times e^{-\frac{(x-t_m)^2}{2\sigma^2}} + \frac{d}{1 + e^{-\frac{(x-t_m)}{2\sigma}}}, \quad (1)$$

where C_0 is the initial CHL concentration, h is the BA, x is the time step, t_m is the BPT, σ is the bloom width, and d represents the residual CHL concentration (Figure 3). This equation is based on the Gaussian function proposed by Yamada and Ishizaka (2006), with the addition of a sigmoid function. As shown in Figure 3, there exists an average CHL difference (d) before and after the bloom in the region during most of spring and summer seasons. Since this feature can cause timing errors of the bloom when using symmetrical normal Gaussian fitting around the bloom peak, sigmoid function has been added. In this curve, the BIT (t_i) was calculated as follows, according to the method of Yamada and Ishizaka (2006):

$$t_i = t_m - 2\sigma \quad (2)$$

In order to isolate the central CHL bloom only as mentioned earlier, we set the possible range of peak timing to during November and December, and the iterative fitting was performed until the minimum variance.

3.3. Relevance of Factors to Interannual Variability in Phenology Metrics

In order to identify how forcings influence the interannual variability in individual phenology metric, multi-linear regression models in the following form were applied to the data using stepwise variable selection:

$$Y = \beta_0 + \beta_1 P_1 + \beta_2 P_2 + \dots + \beta_n P_n + \varepsilon, \quad (3)$$

where Y is the dependent variable, that is, a metric of CHL phenology estimating from the independent variables (predictors), $P_1 \dots P_n$. The parameter β_0 is a constant and $\beta_1 \dots \beta_n$ are the regression coefficients for the predictors, and ε is the error term.

In multilinear regression analysis, it is vital to select the appropriate independent variables, so the predictors for interannual variability in phytoplankton phenology in the central RSP were selected based on the previous studies (refer to section 3.4). In addition, the stepwise variable selection method with F tests was used to select the predictors. Models with and without a particular independent variable were compared using an extra sum of squares F test (Murtaugh, 2009), with $P < 0.05$ as the threshold for the inclusion/exclusion of that predictor. Predictors in a multilinear regression model need to be independent of each other to yield correct results. We tested this for each predictor by calculating the variance inflation factor (VIF), a good indicator of strong correlations between predictors; $VIF < 10$ is considered to indicate no strong relationship between the predictor variables (Myers, 1990). Considering the VIF, we repeatedly ran the model until no variables have the VIF of ≥ 10 .

Furthermore, the proportional reduction of error (PRE) was used to confirm the relative contribution of a predictor to the model using the followings equation (Judd et al., 2011):

$$\text{PRE} = (\epsilon_{\text{total}} - \epsilon_{P_1}) / \epsilon_{\text{total}} \quad (4)$$

where ϵ_{total} is the error in the model computed over all significant independent variables and ϵ_{P_1} is the error in the calculated model after excluding a particular independent variable (P_1). This index allowed the relative contribution of each independent variable (AIRT, SST, Wspd, Wdir, SIC, and PAR) to the total proportional reduction of the error to be calculated.

3.4. Predictor Selection

As previously discussed, predictor selection is an essential part of a multilinear regression analysis. In this study, the potential predictive factors that could influence the interannual variability in each phytoplankton bloom property in the central RSP were selected based on the hypothesis of the previous studies, including the stepwise method.

Both the AIRT and the SST regulate physical constraints such as stratification and mixing, and thus the growth and diversity of phytoplankton, and that they significantly influence phytoplankton metabolism (Toseland et al., 2013). Especially, *P. antarctica* biomass has a strong inverse relationship with water temperature (Liu & Smith, 2012). In addition, turbulent mixing by the winds affects mixed layer formation, with stronger the Wspd producing a deeper mixed layer, resulting in the dominance of *P. antarctica* (Smith & Jones, 2015). The Wdir was also used in this research based on the argument of Nihashi and Ohshima (2015) that the Wdir is strongly correlated with the development of polynya. In addition, sea ice plays a vital role in the iron supply in the RS (Kaufman et al., 2017; Sedwick et al., 2011), and its cover restricts the irradiance availability (Smith et al., 2017). Irradiance (PAR) directly involves the phytoplankton growth (Nelson & Smith, 1991; Smith et al., 2006) and also warms the surface layers by solar insolation. Such warming affects the phytoplankton dynamics by modifying the difference in density between the mixed and deeper layers (Frouin & McPherson, 2012) and melting ice by the positive heat budget (Arrigo, Weiss, & Smith, 1998; Asper & Smith, 2003). The increased SST resulting from strong irradiance is responsible for the enormous expansion of the RSP in the late spring due to a positive heat budget (Arrigo, Weiss, & Smith, 1998; Asper & Smith, 2003). These factors, solely or independently, do not affect the interannual variability in the CHL phenology but have complex interactions between them. Therefore, all of these factors were used together associated with the interannual variability in the CHL phenology in the central RSP, and factors that are not covered in this paper need to be taken into consideration.

In the present study, the use of primary data rather than physical term is to minimize relations between independent variables in the multilinear regression model. Based on the relationship with the phytoplankton dynamics previously mentioned, we selected the SST, AIRT, Wspd, Wdir, SIC, and PAR as possible predictors. We separated values for these variables into monthly data and used to assess differences in the monthly characteristics of each element. Each variable was represented by the variable name with the month, as a numeral, appended; for example, the SST in October was expressed as "SST10."

Table 1

Phenology Metrics Extracted Using the Adjusted Gaussian Fitting. (C_0 : Initial CHL Concentration, h : BA, σ : Bloom Width, t_m : BPT, t_i : BIT, t_t : Bloom Termination Timing)

Period	C_0	d	h	σ	t_m	t_i	t_t	R^2	RMSE
2002/2003	0.07	0.42	0.45	6.74	2002-12-25	2002-12-12	2003-01-08	0.97	0.05
2003/2004	0.00	1.12	4.10	7.13	2003-12-08	2003-11-23	2003-12-22	0.94	0.37
2004/2005	0.07	0.24	2.28	15.62	2004-12-16	2004-11-15	2005-01-17	0.92	0.32
2005/2006	0.00	1.13	4.13	11.30	2005-12-09	2005-11-16	2005-12-31	0.94	0.40
2006/2007	0.00	1.20	4.23	10.31	2006-12-05	2006-11-14	2006-12-26	0.97	0.33
2007/2008	0.00	0.88	5.03	14.08	2007-12-25	2007-11-27	2008-01-22	0.91	0.69
2008/2009	0.04	0.58	1.86	9.97	2008-12-16	2008-11-26	2009-01-05	0.69	0.36
2009/2010	0.00	0.07	7.92	20.92	2009-12-24	2009-11-12	2010-02-03	0.91	1.07
2010/2011	0.00	1.26	8.51	8.79	2010-11-27	2010-11-09	2010-12-15	0.95	0.50
2011/2012	0.09	0.65	2.18	13.46	2011-12-22	2011-11-25	2012-01-18	0.83	0.38
2012/2013	0.03	1.30	3.17	5.27	2012-11-27	2012-11-16	2012-12-07	0.92	0.39
2013/2014	0.00	0.57	2.12	14.35	2013-12-19	2013-11-21	2014-01-17	0.97	0.15
2014/2015	0.04	0.48	6.70	3.72	2014-11-26	2014-11-19	2014-12-04	0.97	0.31
2015/2016	0.00	0.76	4.91	11.36	2015-12-06	2015-11-14	2015-12-29	0.91	0.57
2016/2017	0.00	0.46	6.74	16.66	2016-12-16	2016-11-13	2017-01-18	0.92	0.79

Note. Date is formatted as YYYY-MM-DD. CHL = chlorophyll; BPT = bloom peak timing; BIT = bloom initiation timing; RMSE = root-mean-square error.

4. Results

4.1. Estimation of Phenology Metrics

To assess the interannual variability of the phytoplankton bloom in the central RSP, we estimated the CHL phenology metrics using the adjusted Gaussian curve fitting and calculated the root-mean-square (R^2) values and root-mean-square error of the fitted curves (Table 1 and Figure S2 in the supporting information). The average BA (h) across all seasons was approximately 4.29 mg/m³, ranging from 0.45 mg/m³ in the austral spring-summer 2002/2003 period to approximately 8.51 mg/m³ in the 2010/2011 period. In comparison, Peloquin and Smith (2007) measured the CHL concentration in the central RSP region during 2001–2004. They presented the average CHL concentration of 2.13 and 5.22 mg/m³ in December 2002/2003 and 2003/2004, respectively. Compared with our results, 4.10 mg/m³ during the 2003/2004 period was approximately similar to their result, but the CHL concentration of 0.45 mg/m³ during the 2002/2003 period was considerably underestimated. In 2002–2003, the formation of polynya was very limited due to an iceberg (Arrigo & van Dijken, 2003). As such, the satellite observations were limited, causing a significant discrepancy with field observations. In addition, Sedwick et al. (2011) and Smith et al. (2013) reported CHL concentrations of 1.8–6.0 mg/m³ from 27 December 2005 to 23 January 2006, with an average value of 2.13 mg/m³ between 6 November and 6 December 2006. The average CHL concentration during the 2005/2006 period was approximately 4.13 mg/m³ in the present study, which is in the range suggested by them. Furthermore, Queste et al. (2015) used a sea glider to observe physical and biogeochemical factors around the Ross Bank from 14 December 2010 to 13 January 2011 and reported a maximum CHL concentration of 7 mg/m³; this value was almost similar to the highest CHL concentration (8.50 mg/m³) during the 2010/2011 period observed in the present study, considering the differences between satellite and in situ observations.

The average BIT was in mid-November (17), with the earliest and latest onset of central RSP blooms observed in early November (9, in 2010/2011) and mid-December (12, in 2002/2003), respectively. Averaged over the study period, the BPT was in mid-December (11) (Arrigo & McClain, 1994; Asper & Smith, 1999; Smith, Dennett, et al., 2003). The earliest central RSP bloom peak occurred in the 2014/2015 period, appearing at the end of November (26) (Arrigo & van Dijken, 2004). During that period, the bloom reached its peak within 1 week, the shortest duration over the whole period. The latest blooms peaks were observed in 2002/2003 and 2007/2008 periods, appearing at the end of December (25).

4.2. Interannual Variability in BA in the Central RSP

The factors that affect the BA were investigated with multilinear regression analysis using the predictors selected with the theoretical and statistical methods outlined in section 3.4. The result of multilinear

Table 2
The Result of Multilinear Regression for BA

Predictor	Unstandardized coefficients		Standardized coefficients		<i>t</i> statistic	<i>p</i> value	VIF	PRE	Relative contribution (Reg. var./total var.; %)
	β	Std. error	<i>B</i>						
Wspd10	1.002	0.378	0.512		2.649	$p < 0.05$	1.198	0.351	58.8/36.8
Wdir11	-0.064	0.029	-0.429		2.599	$p < 0.05$	1.198	0.246	41.2/25.8

Note. Model summary: $r = 0.791$, $R^2 = 0.625$, Std. error of the estimate = 1.570, *F* statistics = 10.004, and *p* value < 0.01. BA = bloom amplitude; VIF = variance inflation factor.

regression for the BA showed that both Wspd10 and Wdir11 significantly affected the interannual variability in the BA in the central RSP ($P < 0.05$; Table 2). Both predictors explained 62.5% of the observed variability in the BA; the remaining 37.4% was probably related to other predictors that were not selected due to multicollinearity and to the complexity of the various mechanisms involved. Although the Wspd11 also had a significant impact on the BA within a valid range, it was excluded from the model due to multicollinearity with the Wspd10 ($r > 0.6$; see Figure S1), including the Wdir12. That is, the wind conditions appear to be strongly associated with BA in springtime.

In the model output, the regression coefficient was positive for Wspd10 (unstandardized: 1.00; standardized: 0.51) and negative for Wdir11 (unstandardized: -0.06; standardized: -0.43; Table 2), indicating that enhanced BA is correlated with both strengthened Wspd10 (and also Wspd11) and counterclockwise rotational changes in Wdir11. In addition, given that the prevailing winds in this region blow toward the north (Dale et al., 2017; Nihashi & Ohshima, 2015), we found that BA was enhanced when the wind changed from northeastward (↗) to northwestward (↖) winds. An analysis of the proportional reduction of error showed that Wspd10 explained 58.8% of the variance in the modeled result and 36.8% of the variance in the observed BA, whereas Wdir11 explained 41.2% and 25.8%, respectively.

The observed and modeled variabilities of the BA in the central RSP have steadily increased since 2002 by 0.22 ($P < 0.05$) and 0.25 ($P < 0.01$) $\text{mg}\cdot\text{m}^{-3}\cdot\text{year}^{-1}$, respectively (Figure 4a). This increase is evident each year even excluding the 2002/2003 period, which recorded low biomass associated with an anomalous ice motion caused by the presence of an iceberg in the RS (Arrigo & van Dijken, 2003; Smith, Dennett, et al., 2003). During the increasing trend of BA, the observed BA had its highest values in two successive periods (7.92 mg/m^3 in 2009/2010 and 8.51 mg/m^3 in 2010/2011). The modeled BA simulated the high values observed during the 2009/2010 period, but it did not agree during 2010/2011. This discrepancy was likely due to the inclusion of only Wspd10 as a predictor in the regression model because this was high in 2009/2010 but not in 2010/2011 (Figure 4b). In contrast, the Wspd11 was high both periods, suggesting that this is also an essential factor for the interannual variability in the BA, even though it was excluded from the model. Taken together, the changes in the Wspd and Wdir in October and November were mostly related to the interannual variability in the BA, indicating that the winds over the central RSP contributed significantly to the bloom formation up to the bloom peak.

The BA showed a steady increase, although not statistically significant, before (0.59 $\text{mg}\cdot\text{m}^{-3}\cdot\text{year}^{-1}$) and after (0.13 $\text{mg}\cdot\text{m}^{-3}\cdot\text{year}^{-1}$) the 2009/2010 and 2010/2011 periods when unusually the high BA appeared, while the 3-month averaged Wspd tended to increase before those periods (0.48 $\text{m}\cdot\text{s}^{-1}\cdot\text{year}^{-1}$; $P < 0.10$) and then decrease after them (-0.62 $\text{m}\cdot\text{s}^{-1}\cdot\text{year}^{-1}$; $P < 0.01$). Given that there was a positive relationship between the interannual variabilities in the BA and Wspd, this would suggest that the BA should also have decreased after 2010/2011, associated with the negative trend in the Wspd. However, the BA was slightly enhanced, probably because of the effects of other factors. This inconsistency in the relationship between the Wspd and BA after the 2010/2011 period could

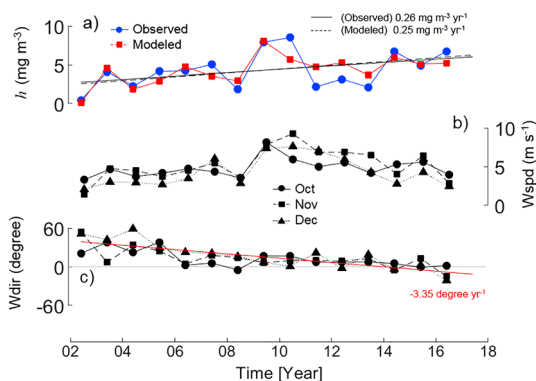


Figure 4. The interannual variability in (a) the observed (blue solid line and circles) and modeled (red solid line and squares) bloom amplitude, (b) Wspd, and (c) Wdir over the central Ross Sea Polynya during October (black solid line and circles), November (black dashed line and squares), and December (black densely dashed line and triangles). In the Wdir, the north and east are 0° and 90° , respectively. The colored lines indicate the linear trends. The shaded zone indicates the time that bloom amplitude appeared unusually high.

Table 3
The Result of Multilinear Regression for BIT

Predictor	Unstandardized coefficients		Standardized coefficients		<i>t</i> statistic	<i>p</i> value	VIF	PRE	Relative contribution (reg. var. /total var.; %)
	β	Std. error	<i>B</i>						
SST11	-17.704	4.306	-0.617		-4.111	<i>p</i> < 0.01	1.048	0.489	61.9/45.9
Wspd10	-3.222	0.999	-0.484		-3.224	<i>p</i> < 0.01	1.048	0.301	38.1/28.3

Note. Model summary: $r = 0.862$, $R^2 = 0.742$, Std. error of the estimate = 4.433, *F* statistics = 14.861, and *p* value < 0.01. BIT = bloom initiation timing; VIF = variance inflation factor.

be related to the change in the Wdir (Figure 4c). Although the trend in the Wdir varied between locations in the RS (Arrigo, Weiss, & Smith, 1998), on average across the study area for 15 years, it showed a statistically significant monotonic change of -3.35° per year ($P < 0.01$).

4.3. Variation in BIT and BPT

4.3.1. Bloom Initiation

In the multilinear regression model for the BIT in the central RSP, the significant factors that explained the variation in the BIT within the valid range were the SST11 and Wspd10 ($P < 0.01$; Table 3). These two predictors explained up to 74.2% of the observed total variation in the BIT; the SST11 explained 61.9% of the modeled variation and 45.9% of the observed variation, and the Wspd10 explained 38.1% and 28.3% of the variations, respectively. The regression coefficients of both predictors were negative, indicating that a higher SST11 and increased Wspd10 resulted in an earlier onset of the blooms in the central RSP. Although the BIT model suggested that only the SST11 and Wspd10 were remarkable, the SST12 and Wspd11 also showed correlations with the variability in the BIT ($r = -0.81$ and -0.64 , respectively; Figure S1); however, these were excluded from the model due to multicollinearity.

Unlike the BA, the interannual variability in the BIT showed no significant trend ($P > 0.10$). However, it was clear that the BIT was delayed in the phase during which the Wspd10 and SST11 were increased, and the delayed BIT occurred during the phase with the reduced Wspd and SST (Figure 5a). Based on this relationship, the impact of the Wspd and SST on the BIT was quantitatively estimated, taking into account both their contribution and variability, as shown in Figure 5b.

In particular, BIT was about 18 days earlier in the 2003/2004 period than in the 2002/2003 period (observed: -19 days; modeled: -16 days), and the early bloom occurred around the same time in the 2008/2009 and 2009/2010 periods (observed: -15 days; modeled: -20 days). Between the 2002/2003 and 2003/2004 periods, the Wspd increased by about 1.39 m/s, and the SST showed an increase of 0.68 °C. In addition, the Wspd and SST increased by 4.68 m/s and 0.33 °C, respectively, between the 2008/2009 and 2009/2010 periods. The contributions of the Wspd and SST during the 2008/2009 and 2009/2010 periods were 10% higher than those of 2002/2003 and 2003/2004, suggesting that although there was a substantial increase in the Wspd, the increase in the SST with a more significant contribution to the BIT model was half the level, leading to a similar change in the BIT. In contrast, the BIT for 2006/2007 and 2010/2011 was instead delayed (approximately 11 and 12 days, respectively). Between the 2006/2007 and 2007/2008 periods, the Wspd10 decreased by about 0.36 m/s and the SST11 decreased by 0.43 °C. The decrease in the Wspd10 and the SST11 between the 2010/2011 and 2011/2012 periods were 0.97 m/s and 0.31 °C, respectively, a significantly more significant decrease in the Wspd compared to the earlier period. In addition, there was a high correlation between the interannual variability in the BIT and the effect level calculated from the Wspd10 and SST11 and presented in

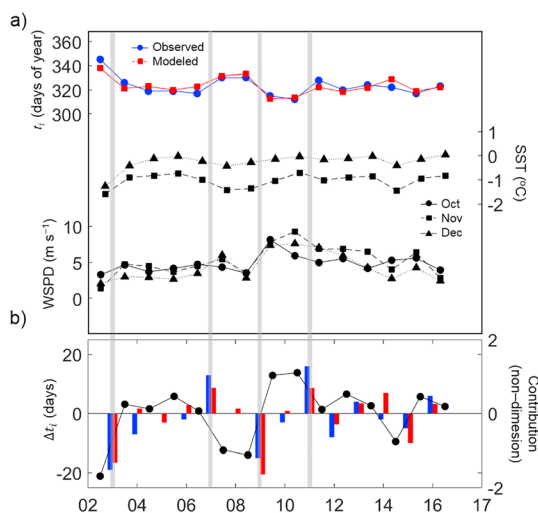


Figure 5. (a) Interannual variabilities in the observed (blue circles) and modeled (red squares) BIT and SST, and Wspd in the central Ross Sea Polynya during October (black solid line and circles), November (black dashed line and squares) and December (black densely dashed line and triangles). (b) The time series of the observed (blue bars) and the modeled (red bars) BIT changes and the combined effect of SST and Wspd (black solid line and circles, refer to the script). The y axis on the left represents the year-to-year differences in both the observed and the modeled BIT, and the y axis on the right represents the ratio of the normalized values of Wspd10 and SST11 (i.e., $0.381 \times \text{normalized Wspd10} + 0.619 \times \text{normalized SST11}$), showing quantitatively the effect of both predictors simultaneously. BIT = bloom initiation timing; SST = sea surface temperature; Wspd = wind speed.

Figure 5b ($R = 0.95$); this resulted in the earlier BIT when the Wspd10 and the SST11 increased simultaneously, and the later BIT when they both decreased.

4.3.2. Bloom Peak

Unfortunately, there were no significant predictors for the interannual variability in the BPT in the central RSP, at least on the interannual time scale. This fact showed that the BPT was either probably influenced to a low extent by the factors selected in this study on the interannual time scale or was affected by factors not included in the model. However, the BPT showed moderate positive ($r = 0.56$) and negative ($r = -0.45$) correlations with the interannual variabilities in the BIT and the BA, respectively, suggesting that an earlier BIT and higher BA are related to an earlier bloom peak. This relationship may be due to the intrinsic variability of the bloom or indirectly by factors that have influenced the BA and BIT. In the BPT model implemented with the BA and BIT as new predictors, we found that the BIT had a significant impact on the BPT, accounting for about 56.2% ($P < 0.05$) of the interannual variability in the BPT (data not shown). Although the BA was also a correlation with BPT ($R = -0.45$, $P < 0.10$), BA shows a slightly lower relationship and significance than the relationship with the BIT ($R = 0.56$, $P < 0.05$). In addition, only the BIT is likely to be selected as a significant result because the BIT and BA were not completely independent factors ($R = -0.66$). Consequently, considering BA in the description, their correlations indicated that an earlier BPT occurs when the bloom starts earlier, and a more abundant bloom appears, and vice versa. However, it is challenging to elucidate the detailed mechanism with this limited information.

5. Discussion

5.1. Wdir Changes for BA

The interannual variability in the BA might significantly influence by the Wspd and Wdir in spring and summertime (Table 2) and responded to the enhanced Wspd events and progressive change in the Wdir (Figure 4). In particular, the Wdir changes seem to be strongly associated with the overall trend in the BA. Conventionally, the wind is considered as the primary contributor for polynya formation and expansion in the RS (Nihashi & Ohshima, 2015; Park et al., 2018; Zwally et al., 1985). In particular, Nihashi and Ohshima (2015) suggested that the Wdir could play a significant role in their formation and maintenance because it is highly correlated to the area of polynyas. In addition, Park et al. (2018) argued that meridional and zonal winds in the RS play a different role in the expansion of the summertime polynya. They also noted a strong correlation between the nonlinearities of the RSP expansion and the zonal winds, resulting in a climate shift in the 1990s. The weakened zonal wind is in line with the recent change in the WDIR suggested in this analysis. Consequently, we speculated that the recent Wdir (with weakened zonal winds), which favored polynya expansion, may have further strengthened the summer RSP expansion. In succession, the unprecedented expansion of polynya could lead to a higher BA (Reddy & Arrigo, 2006).

In order to study the causes and effects of the changes in the Wdir, we suggested the climatological wind conditions, SIC patterns, and the consequent distribution of CHL in the RS as shown in Figure 6. We separated the two periods early (2002/2003, 2003/2004, and 2004/2005) and late (2014/2015, 2015/2016, and 2016/2017) phases to isolate the specific effect of the Wdir from another factor, since these two periods could be characterized by the similar average Wspd (early phase: 3.35 m/s, late phase: 4.15 m/s) and significantly different mean Wdir (early phase: 40.95° , late phase: -4.94°). In addition, these three-season averages were to eliminate the effects of an exceptional event in a particular year.

During the early phase, the atmospheric circulation pattern included a jet associated with a steep pressure gradient in a north-south direction and a pressure minimum over the *Cape Colbeck* (about 982 hPa). Along the existence of the jet originating from the interior of the continent, the wind blows northwestward across the RIS, turning northward near the coastal margin, and then northeastward over the sea (Figure 6a). Because the study region belongs to a transition zone where the wind starts to change direction from the north to the northeast, the averaged zonal wind component in the central RSP has a positive value, (i.e., representing a weak northeastward wind). As such, the potential ice-free zone (for which mean SIC is less than the 60% threshold, with 100% SIC in October and entirely ice free in December) might be formed by Ekman-induced ice drift along the jet confined to the western RS (Figure 6c). The synoptic pattern of

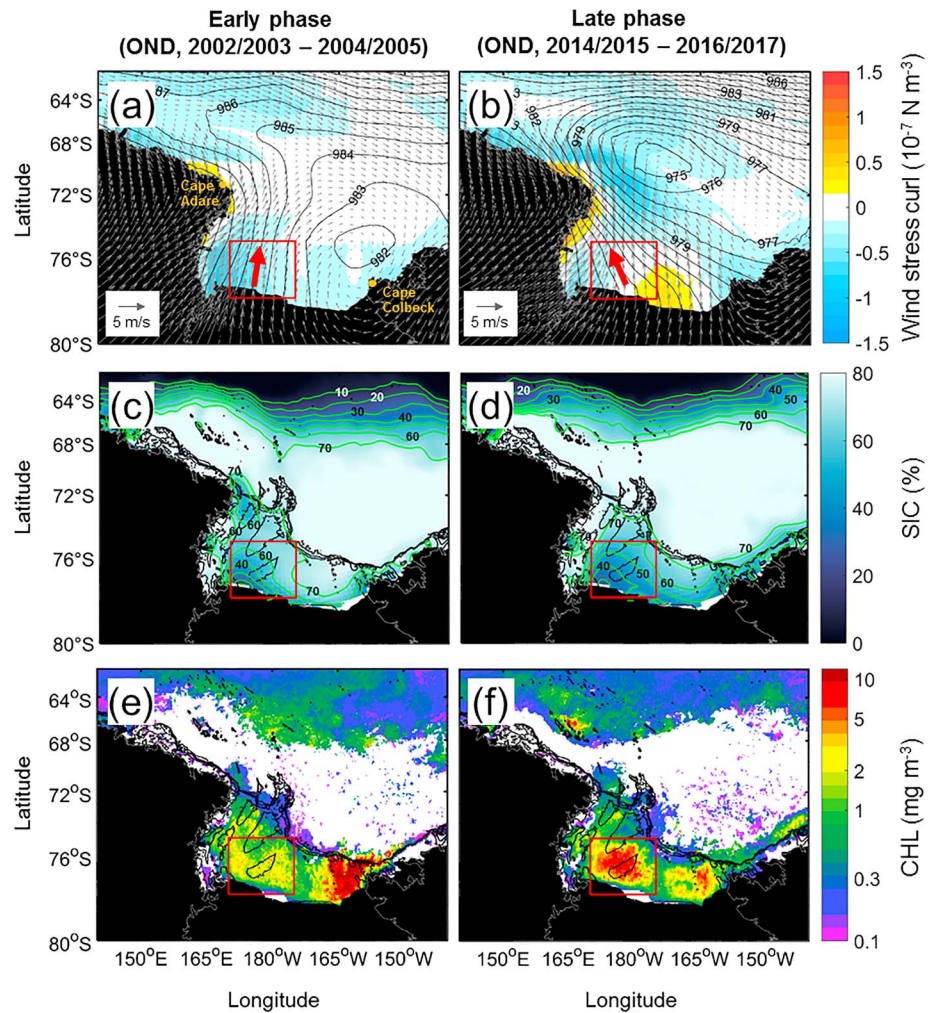


Figure 6. (a, b) The averaged wind fields (vector), mean sea level pressure (contour), and wind stress curl (colored) from October, November, and December (OND). (c, d) The averaged sea ice concentration (SIC) during November and December. The green contour indicates the ice concentration with interval 10% ranged from 10–70%. (e, f) The averaged chlorophyll (CHL) concentration during austral spring and summer. The left and right panels are the results for three years during early (2002/2003–2004/2005) and late (2014/2015–2016/2017) phases, respectively. The red box represents the study area (the central Ross Sea Polynya).

winds during the end phase involves a robust cyclone over the northern RS and stronger wind near *Cape Adare* than that during the early phase (Figure 6b). There was a pressure minimum of 975 hPa over the RS (near 175°W, 68°S) and a steep pressure gradient throughout the domain, resulting in stronger winds, except where the pressure minimum was located (Figure 6a). In addition, the jet, which was stronger than that during the early phase was fully aligned between *Cape Colbeck* and *Cape Adare*, which stretch from the eastern RIS to the northward. This jet is likely to have strengthened the wind stress in the most eastern RS coasts because it was broader and stronger than that during the early phase (Figure 6b). The strengthened wind stress over the periphery of the eastern RIS could eventually result in relatively low SIC in the ocean along the northern part of the RIS (Figure 6d), through the Ekman-induced ice drift.

The most significant difference between the two phases associated with the synoptic pattern was in the local wind stress curl (Figures 6a and 6b). Positive wind stress curl implies the divergent ice drift induced by increased surface stress and upwelling velocity (Kim et al., 2017). During the early phase of the study (at $<0.5 \times 10^{-7} \text{ N/m}^3$), the positive stress curl is confined to a small part of the coastal areas near the *Cape Adare* (165–180°W, 72–75°S), whereas the areas with the intense negative curl (i.e., with convergence and downwelling) followed the jet beginning in the western RIS. During the late phase, the positive wind

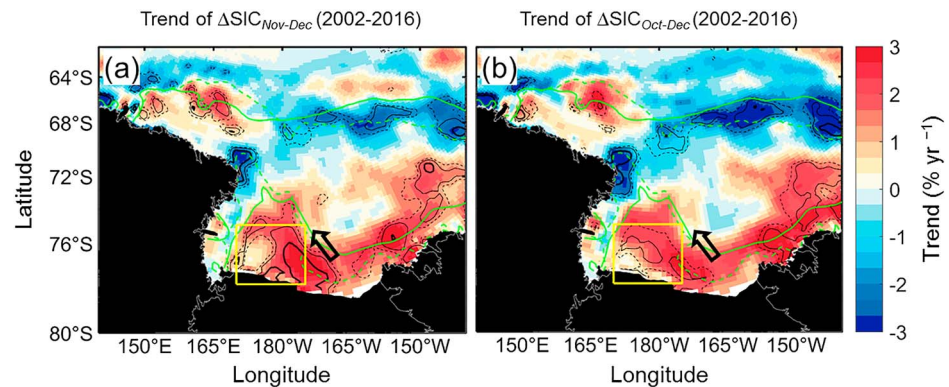


Figure 7. Trends of sea ice loss during the entire study period (a) between November and December and (b) between October and December. The background color indicates the trend of sea ice loss, and the solid green lines are the contour of sea ice concentration (SIC) 60% during the late phase. The confidence interval of 90% (thin dotted line), 95% (thin solid line), and 99% (thick solid line). The yellow box represents the region of interest.

stress curl near *Cape Adare* was higher than that during the early phase (Coggins et al., 2014; Coggins & McDonald, 2015), and there was also a robust negative wind stress curl at the western boundary of the pressure minimum. The wind stress curl distributions during the two phases showed a substantial difference over the eastern RIS coast. According to the alignment and intensity of the jet, the stress curl for the region during the early phase did not show any distinctive feature, but there was a high positive curl of nearly $0.5 \times 10^{-7} \text{ N/m}^3$ during the late phase. The robust transport induced by the enhanced wind stress could result in vigorous ice drifts along the Wdir of the surrounding region, exposing the sea surface over a wider area (Figure 6d). The positive curl value due to the combination of wind and sea ice in a polynya (Kim et al., 2017) generally suggests that the expansion of regions with potential ice-free states within the regions of interest during the late phase was increased due to a strong pressure gradient (i.e., a stronger Wspd), which was broader than that during the early phase; these changes could host the high biomass abundance in the study area as the light condition improved (Montes-Hugo & Yuan, 2012; Reddy & Arrigo, 2006). In fact, unlike the early phase when the high CHL was present only in the eastern region of the RS shelf (Figure 6e), the high CHL ($>5 \text{ mg/m}^3$) aggregates were found in the study area during the late phase (Figure 6f).

As a result, the wind pattern changes are likely to influence the distribution of the sea ice, in turn, the BA trend. Therefore, analysis of the trend in sea ice is needed. To investigate the trend in sea ice during the entire study period, we illustrated the distribution of trends of difference in the SIC between November–December and October–December, as shown in Figure 7. This ice removal trend focused from October, when ice begins to be removed, to December, when BA appears on average. The ice removal has significantly increased over the southern RS, especially in the region with the positive wind stress curl shown in Figure 6 b. Such removal is particularly evident between November and December. This positive trends extended northwest from the coast; this was reasonably consistent with the changes in the Wdir. This alignment was also evident in the rate of the ice removal between October and December (Figure 7b), but with weak significance. The positive trends observed over most of the southern coast is likely to be associated with the recent alignment of the jet over the RS (Figures 6b). The recently reinforced jet seems to have contributed to extending the 60% SIC contour further north over most of the southern coast.

5.2. Regionally Asymmetric Trend Pattern of CHL at BPT

The increased sea ice removal in spring and summertime (Figure 7) may result in the distinct differences in biomass abundance observed between the early and late study periods (Figures 6e and 6f). However, while the ice removal tends to increase throughout the southern RS, unexpectedly, the trends of CHL at the BPT show a substantial spatial difference (Figure 8). This difference was most pronounced across the Ross Bank, where the bloom peak tended to increase in the western part of the feature (near 176°W , 75.5°S ; maximum $+0.9 \text{ mg}\cdot\text{m}^{-3}\cdot\text{year}^{-1}$ at the 90% confidence level), whereas it tended to decrease sharply on the eastern side (near 180°W , 77.5°S ; maximum $-1.2 \text{ mg}\cdot\text{m}^{-3}\cdot\text{year}^{-1}$). Within the statistically significant range, the average

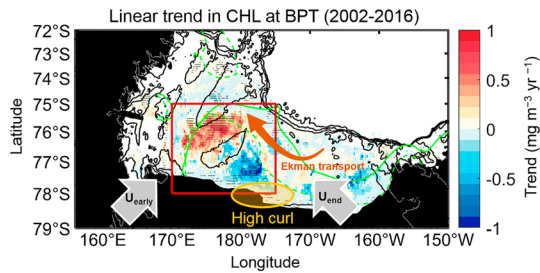


Figure 8. The linear trend map of the chlorophyll (CHL) at the bloom peak timing (BPT) during 2002–2016. The red box is the study area, and the gray arrows are the W_{dir} during the early (U_{early}) and end (U_{end}) phases. The green solid and dashed lines represent the contour lines of 60% ice concentration during the early and end phases, respectively. The orange elliptical shape is a region with the high positive wind stress curl (refer to Figures 6 and 7). The dark orange curved arrow suggests the direction of the expected Ekman transport.

positive trend was $+0.5 \text{ mg}\cdot\text{m}^{-3}\cdot\text{year}^{-1}$, and the average negative trend was $-0.2 \text{ mg}\cdot\text{m}^{-3}\cdot\text{year}^{-1}$. This suggested that, although the maximum value of the negative trend was more significant than that of the positive trend, the region with the significant positive trend was about 1.95 times larger than the region with the negative trend. This dominance of positive trends within the study area was likely to be associated with the overall increasing trend in the BA.

The asymmetric trend in the CHL at BPT between the eastern and western sides of the Ross Bank can be interpreted according to the hypothesis suggested by Reddy and Arrigo (2006). They noted that the pattern of the surface phytoplankton distribution is affected both by changes in the mixed layer depth and by the lateral advection of surface water. In general, during the austral spring and early summer in the RS, bloom formation in areas with a deepened mixed layer depth due to wind-induced mixing is generally restricted by a lack of light (Smith & Jones, 2015). Conversely, enhanced light conditions in areas with shallow mixed layer depths result in increased phytoplankton growth and, in turn, higher CHL concentrations. This relationship is especially evident in environments where there has already been considerable stratification due to the recent removal of sea ice. The recent increase in wind stress curl around the study area (Figures 6b and 7), along the southeastern coastal area, could be expected to result in significant mixing in these areas. This direct stress had the potential to constrain the bloom in the eastern region of Ross Bank through the limitation of light with the increase in the mixed layer depth. In addition, based on the ocean circulation pattern in the southwestern RS reported by Reddy and Arrigo (2006), the flow on the Ross Bank moves to the northwest from the eastern flank and can be characterized as a junction with the relatively cold, fresh water that flows southward along the trough between Pennell Bank and Ross Bank. During the early period of the study, the CHL could be advected northeastward from the less developed RSP by the relatively weak northeastward winds, and the CHL advection flowing upstream against the geostrophic current may have become concentrated over a small area in the east of the Ross Bank. However, the strong northwestward winds associated with the strong jet aligned in the northwest-southeast direction, induced by the recently changed synoptic pattern (Figure 6b), might result in a horizontal advection in the northwest direction across the entire southern RS, probably contributing to the forming westward spread of the bloom. The recent westward spread of the bloom was larger than the bloom that developed earlier east of the Ross Bank with the improved light availability because of the wider potential ice-free zone (Figure 6b); this was responsible for the continued increase in the interannual variability in the BA. The growth of phytoplankton over the trough between the Ross Bank and the Pennell Bank is likely restricted by the inflow of cold, fresh water from outside of the shelf; this region of low CHL is maintained from year to year (Line 3 in Reddy & Arrigo, 2006). Nevertheless, it can be inferred from the large blooms that covered the area during the last two seasons that these were forced into the area by the transport of surface waters caused by strong winds. These results are inconsistent with those of Reddy and Arrigo (2006), who proposed that the horizontal flow of CHL in the RS was dominated by the geomorphic flow and that advection by Ekman dynamics was insignificant. This suggests that the recent change in Ekman dynamics caused by the change in the synoptic pattern over the RS could raise its contribution to advection in the surface water in this region.

5.3. Factors That Determine BIT

The BIT did not show a significant trend on a long time scale. However, it seemed to be heavily influenced by SST and Wspd (Table 3). In particular, it was earlier when SST or Wspd increases. The BIT in the RS has traditionally been thought to be associated with increased irradiance, the vertical stability of the water mass, and the iron supplied by ice melt (Queste et al., 2015; Sedwick & DiTullio, 1997; Smith & Comiso, 2008; Smith & Gordon, 1997). In particular, Reddy et al. (2007) investigated the processes that drive the dynamics of the summer RSP using a coupled ice/ocean model and concluded that the advection of sea ice resulting from wind stress plays a primary role in summer polynya formation. They also suggested that the formation and expansion of the summer RSP were primarily related to heat entrainment reducing the rate of sea ice formation rather than increasing sea ice melting. In addition,

Table 4
The Correlation Between the Interannual Variability in the BIT and the Timing When the Averaged SIC in the Central RSP Recorded a Certain Threshold (RSP Onset Timing)

SIC threshold (%)	<i>r</i> with opening time
0	NaN
10	0.18
20	0.27
30	0.27
40	0.44
50	0.74**
60	0.56*
>70	NaN

Note. The threshold value was set from 0% to 100% with 10% interval. BIT = bloom initiation timing; SIC = sea ice concentration; RSP = Ross Sea Polynya.

* $p < 0.05$. ** $p < 0.01$.

they noted that the advection of sea ice being induced by the synoptic wind events associated with variations in atmospheric pressure. Queste et al. (2015) suggested that strong winds could weaken the vertical stabilization of the water layer, thereby resulting in late blooms and that a decrease in the Wspd could accelerate stratification and increase biomass abundance. Furthermore, Arrigo, Weiss, and Smith, (1998) suggested that the prolonged presence of sea ice allowed rapid phytoplankton growth and an early bloom through reduced vertical mixing and the advection of surface waters resulting from the weakened wind stress. However, these arguments by Arrigo, Weiss, and Smith, (1998) and Queste et al. (2015) were not consistent with the results of the present study, which showed that the bloom onset was earlier when Wspd increased. During the October to November when the blooms mostly start (Table 1), there is generally still a weak stratification in the RSP (Arrigo et al., 2003), and the ice drift has a greater effect on the sea ice distribution rather than the removal of ice by ice melting in the RSP (Arrigo & McClain, 1994). Therefore, a vigorous

ice drift induced by strong winds might expose a greater area of the ocean surface to the atmosphere, reducing light restrictions; in turn, this could result in an earlier bloom.

In the BIT model, the contribution of the SST was twice that of the Wspd (Table 3), indicating that the SST was a more critical factor for the interannual variability in the BIT than the Wspd. Alongside the mechanism just described in which a strong Wspd enables earlier BITs through advancing the timing of RSP expansion, the water temperature is also a physical factor that can regulate to such timing of RSP expansion (Asper & Smith, 2003). The onset of polynya could be influenced by the advection of the relatively warm ($\sim 0.5^\circ\text{C}$) water mass of the Antarctic Circumpolar Current flowing into the shelf from the continental slope and this warm water provides a source of heat and facilitates to melt ice (Asper & Smith, 2003; Jacobs & Comiso, 1989; Markus, 1999). The positive heat budget in the region likely results in the significant expansion of the RSP in late spring and, in turn, enlarges the phytoplankton bloom (Arrigo, Weiss, & Smith, 1998; Asper & Smith, 2003). In addition to such source that can affect the SST, a surface heating on the exposed sea surface can be another thermal source. In particular, it is remarkable that the Wspd (October) and SST (November) in different months are related to the variation in the BIT. Although there may be limitations in interpreting statistical methods alone, it likely suggests that the Wspd first affects the BIT and then the SST affects it. Then, it can be assumed that a vigorous ice drift by a strong Wspd causes an earlier polynya expansion, which in turn can accelerate a surface warming through solar insolation. Then, a shoaling of the mixed layer driven by surface heating promotes optimal irradiance condition, resulting in the earlier onset of the bloom (Coale et al., 2005; Marchese et al., 2017). The consequent expansion in the RSP induced by the two predictors is probably the primary mechanism that determines the onset of the bloom in the central RSP. To quantitatively demonstrate that the expansion of open water associated with the SST and Wspd is related to the BIT, we calculated the interannual variability in the timing of recording a specific SIC value (with 10% interval) within the study area and calculated the correlation between this and the interannual variability in the BIT (Table 4). As such, there was a high correlation of about 0.74 ($P < 0.01$) between them when the mean SIC in the study area was 50%, which is substantial evidence that the timing of opening strongly correlated with the BIT.

6. Conclusions

In the present study, we investigated the characteristics of a representative CHL phenology for the central RSP by determining annual CHL phenology metrics over the 15 years from 2002 to 2017 based on satellite ocean color data using the adjusted Gaussian function method. We also analyzed the interannual variabilities of the bloom phenology metrics, including the BA, BIT, and BPT. In addition, we used a multilinear regression analysis to examine how variations in environmental forcings were associated with variations in the bloom properties. Predictors were selected for inclusion in the models based on hypotheses of previous studies and using the stepwise method.

Our results show that the interannual variability in the BA appeared to be related to only the components of the winds (Table 2); the BA has a positive (0.51) and negative (−0.43) relationship with the Wspd10 and the Wdir11, respectively. The recent increasing trend of the BA probably resulted from the change of wind over the central RSP driven by the modified synoptic pressure pattern (Figures 6a and 6b) and the alteration of sea ice condition by the changing winds (Figures 6c and 6d). In particular, the changing winds increased sea ice loss during the austral spring and early summer over most of the southern coast of the RS (Figure 7). The increased open water formation resulting from the ice loss probably improved the light availability for the phytoplankton growth, in turn, caused the increasing trend in the BA (Figures 4, 6e, and 6f). However, the trend in the maximum CHL concentration showed the symmetry of the trends, centered on the Ross Bank (Figure 8a). In particular, the western part of the Ross Bank showed the high CHL over the last 2 years (Figure 8b); this is probably related to the growing role of Ekman dynamics associated the recent change in synoptic winds.

The statistical model results show that BIT is a function of SST and Wspd (Table 3). In particular, the Wspd10 and the SST11 were selected as the significant predictors for determining the interannual variability in the BIT, which can be inferred as the effect of SST following the impact of Wspd. This relationship showed that an earlier BIT was probably associated with the increases in the SST and Wspd, and vice versa (Figure 5). The enhancement of ice drift resulted from the increase in the Wspd could open the central RSP much earlier (Bromwich et al., 1992) because the central RSP is primarily dominated by ice drift rather than ice melt in October and November when the BIT appeared (Arrigo & McClain, 1994; Reddy et al., 2007). As such, once the area of the exposed surface increases by the enhanced Wspd10, the increased surface water temperature by more solar insolation can accelerate the opening (Queste et al., 2015; Sedwick & DiTullio, 1997; Smith & Comiso, 2008; Smith & Gordon, 1997). There was a significant correlation between the timing of reaching a specific mean SIC value in the study area and the interannual variability in the BIT (Table 4), supporting that the onset timing of the RSP expansion is related to the BIT on the interannual time scale.

No significant predictors for the interannual variability in the BPT were found in this study. However, the BPT was related to changes in the BIT ($R = 0.56$) and BA ($R = -0.45$). The initial determination of the BIT and the BA according to the physical environments could play an intricate role in the determination of the BPT, which thought to be related to iron depletion in the present study. We concluded that the BA and the BIT were probably related to the extent and onset of the polynya expansion, respectively. Given the relationship between the BPT and them, an enhanced and earlier of the RSP expansion probably result in the earlier BPT in the central RSP.

The current study presented an overview of the relationship between the bloom characteristics and the factors based on the statistical approach, highlighting the mechanisms that generate such a relationship. Most mechanisms have been presented in many previous studies, but we believe that this statistical approach alone is encouraging in that the relationship between the bloom and the physical environment can be calculated. However, this study tends to rely solely on statistics and needs attention to its consequences. In addition, the mechanism of the recently changed central RSP bloom presented in this study has been focused on the probability of occurrence based on physical environment change. Therefore, more detailed studies are required to demonstrate the mechanism.

References

- Arrigo, K. R., & McClain, C. R. (1994). Spring phytoplankton production in the western Ross Sea. *Science*, *266*(5183), 261–263. <https://doi.org/10.1126/science.266.5183.261>
- Arrigo, K. R., & van Dijken, G. L. (2003). Phytoplankton dynamics within 37 Antarctic coastal polynya systems. *Journal of Geophysical Research*, *108*(C8), 3271. <https://doi.org/10.1029/2002JC001739>
- Arrigo, K. R., & van Dijken, G. L. (2004). Annual changes in sea-ice, chlorophyll a, and primary production in the Ross Sea, Antarctica. *Deep-Sea Research Part II: Topical Studies in Oceanography*, *51*(1–3), 117–138. <https://doi.org/10.1016/j.dsr2.2003.04.003>
- Arrigo, K. R., van Dijken, G. L., & Bushinsky, S. (2008). Primary production in the Southern Ocean, 1997–2006. *Journal of Geophysical Research*, *Oceans*, *113*(C8), 1997–2006. <https://doi.org/10.1029/2007JC004551>
- Arrigo, K. R., van Dijken, G. L., & Strong, A. (2015). Environmental controls of marine productivity hot spots around Antarctica. *Journal of Geophysical Research: Oceans*, *120*, 1–22. <https://doi.org/10.1002/2015JC010888>. Received
- Arrigo, K. R., Weiss, A. M., & Smith, W. O. (1998). Physical forcing of phytoplankton dynamics in the southwestern Ross Sea. *Journal of Geophysical Research*, *Oceans*, *103*(C1), 1007–1021. <https://doi.org/10.1029/97JC02326>
- Arrigo, K. R., Worthen, D. L., & Robinson, D. H. (2003). A coupled ocean-ecosystem model of the Ross Sea: 2. Iron regulation of phytoplankton taxonomic variability and primary production. *Journal of Geophysical Research*, *108*(C7), 3231. <https://doi.org/10.1029/2001JC000856>

Acknowledgments

This research was supported by the “Ecosystem Structure and Function of Marine Protected Area (MPA) in Antarctica” project (PM18060), funded by the Ministry of Oceans and Fisheries (20170336), Korea and also by the National Research Foundation of Korea (NRF) Grant funded by the Korea government (MSIP; NRF-2018R1A2B2006555). The Moderate Resolution Imaging Spectroradiometer (MODIS) chlorophyll-a concentration data are provided by the Ocean Biology Processing Group at the National Aeronautics and Space Administration, from their website (<http://oceancolor.gsfc.nasa.gov>). The daily Optimum Interpolation SST data and NCEP reanalysis data were provided by the NOAA, USA (<https://www.ncdc.noaa.gov/>). The sea ice concentration data were derived from the Special Sensor Microwave Imager and the Special Sensor Microwave Imager/Sounder passive microwave radiometer data sets, provided by the National Snow and Ice Data Center (<http://nsidc.org/data/nsidc-0051>). We used the Coupled Model Intercomparison Project Phase 5 (CMIP5) model simulation output obtained from the Asia-Pacific Data Research Center (<http://apdrc.soest.hawaii.edu>).

- Asper, V. A., & Smith, W. O. Jr. (1999). Particle fluxes during austral spring and summer in the southern Ross Sea, Antarctica. *Journal of Geophysical Research*, *104*(C3), 5345–5359. <https://doi.org/10.1029/1998JC900067>
- Asper, V. L., & Smith, W. O. (2003). Abundance, distribution and sinking rates of aggregates in the Ross Sea, Antarctica. *Deep-Sea Research Part I: Oceanographic Research Papers*, *50*(1), 131–150. [https://doi.org/10.1016/S0967-0637\(02\)00146-2](https://doi.org/10.1016/S0967-0637(02)00146-2)
- Banzon, V., Smith, T. M., Liu, C., & Hankins, W. (2016). A long-term record of blended satellite and in situ sea surface temperature for climate monitoring, modeling and environmental studies. *Earth System Science Data Discussions*, *8*(January), 1–13. <https://doi.org/10.5194/essd-2015-44>
- Boyd, P. W. (2002). Environmental factors controlling phytoplankton processes in the Southern Ocean. *Journal of Phycology*, *38*(5), 844–861. <https://doi.org/10.1046/j.1529-8817.2002.t01-1-01203.x>
- Boyd, P. W., Arrigo, K. R., Strzepek, R., & Van Dijken, G. L. (2012). Mapping phytoplankton iron utilization: Insights into Southern Ocean supply mechanisms. *Journal of Geophysical Research, Oceans*, *117*(C6), 1–18. <https://doi.org/10.1029/2011JC007726>
- Bromwich, D. H., Carrasco, J. F., & Stearns, C. R. (1992). Satellite observations of katabatic-wind propagation for great distances across the Ross Ice Shelf. *Monthly Weather Review*, *120*(9), 1940–1949. [https://doi.org/10.1175/1520-0493\(1992\)120<1940:SOOKWP>2.0.CO;2](https://doi.org/10.1175/1520-0493(1992)120<1940:SOOKWP>2.0.CO;2)
- Cavalieri, D. J., Parkinson, C. L., Gloersen, P., & Zwally, H. J. (1996). *Sea ice concentrations from Nimbus-7 SMMR and DMSP SSM/I-SSMIS passive microwave data, version 1*. Boulder, CO, USA: National Snow and Ice Data Center.
- Coale, K. H., Gordon, R. M., & Wang, X. (2005). The distribution and behavior of dissolved and particulate iron and zinc in the Ross Sea and Antarctic circumpolar current along 170°W. *Deep-Sea Research Part I: Oceanographic Research Papers*, *52*(2), 295–318. <https://doi.org/10.1016/j.dsr.2004.09.008>
- Coale, K. H., Wang, X., Tanner, S. J., & Johnson, K. S. (2003). Phytoplankton growth and biological response to iron and zinc addition in the Ross Sea and Antarctic Circumpolar Current along 170°W. *Deep Sea Research Part II: Topical Studies in Oceanography*, *50*(3–4), 635–653. [https://doi.org/10.1016/S0967-0645\(02\)00588-X](https://doi.org/10.1016/S0967-0645(02)00588-X)
- Coggins, J. H. J., & McDonald, A. J. (2015). The influence of the Amundsen Sea Low on the winds in the Ross Sea and surroundings: Insights from a synoptic climatology. *Journal of Geophysical Research: Atmospheres*, *120*, 2167–2189. <https://doi.org/10.1002/2014JD022830>
- Coggins, J. H. J., McDonald, A. J., & Jolly, B. (2014). Synoptic climatology of the Ross Ice Shelf and Ross Sea region of Antarctica: K-means clustering and validation. *International Journal of Climatology*, *34*(7), 2330–2348. <https://doi.org/10.1002/joc.3842>
- Dale, E. R., McDonald, A. J., Coggins, J. H. J., & Rack, W. (2017). Atmospheric forcing of sea ice anomalies in the Ross Sea polynya region. *The Cryosphere*, *11*(1), 267–280. <https://doi.org/10.5194/tc-11-267-2017>
- Di Lorenzo, E., & Ohman, M. D. (2013). A double-integration hypothesis to explain ocean ecosystem response to climate forcing. *Proceedings of the National Academy of Sciences*, *110*(7), 2496–2499. <https://doi.org/10.1073/pnas.1218022110>
- Foukal, N. P., & Thomas, A. C. (2014). Biogeography and phenology of satellite-measured phytoplankton seasonality in the California current. *Deep-Sea Research Part I: Oceanographic Research Papers*, *92*, 11–25. <https://doi.org/10.1016/j.dsr.2014.06.008>
- Frouin, R., & McPherson, J. (2012). Estimating photosynthetically available radiation at the ocean surface from GOCI data. *Ocean Science Journal*, *47*(3), 313–321. <https://doi.org/10.1007/s12601-012-0030-6>
- Jacobs, S. S., & Comiso, J. C. (1989). Sea ice and oceanic processes on the Ross Sea continental shelf. *Journal of Geophysical Research*, *94*(C12), 18195. <https://doi.org/10.1029/JC094iC12p18195>
- Ji, R., Edwards, M., MacKas, D. L., Runge, J. A., & Thomas, A. C. (2010). Marine plankton phenology and life history in a changing climate: Current research and future directions. *Journal of Plankton Research*, *32*(10), 1355–1368. <https://doi.org/10.1093/plankt/fbq062>
- Jones, R. M., & Smith, W. O. (2017). The influence of short-term events on the hydrographic and biological structure of the southwestern Ross Sea. *Journal of Marine Systems*, *166*, 184–195. <https://doi.org/10.1016/j.jmarsys.2016.09.006>
- Judd, C. M., McClelland, G. H., & Ryan, C. S. (2011). *Data analysis: A model comparison approach (Second)*. New York: Routledge. Retrieved from https://books.google.com.my/books?id=JDT_ngEACAAJ, <https://doi.org/10.4324/9780203892053>
- Kalnay, E., Kanamitsu, M., Kistler, R., Collins, W., Deaven, D. G., Gandin, L. S., et al. (1996). The NCEP NCAR 40-year reanalysis project. *Bulletin of the American Meteorological Society*, *77*(3), 437–471. [https://doi.org/10.1175/1520-0477\(1996\)077<0437:TNYRP>2.0.CO;2](https://doi.org/10.1175/1520-0477(1996)077<0437:TNYRP>2.0.CO;2)
- Kaufman, D. E., Friedrichs, M. A. M., Smith, W. O., Hofmann, E. E., Dinniman, M. S., & Hemmings, J. C. P. (2017). Climate change impacts on southern Ross Sea phytoplankton composition, productivity, and export. *Journal of Geophysical Research: Oceans*, *122*, 2339–2359. <https://doi.org/10.1002/2016JC012514>
- Kaufman, D. E., Friedrichs, M. A. M., Smith, W. O., Queste, B. Y., & Heywood, K. J. (2014). Biogeochemical variability in the southern Ross Sea as observed by a glider deployment. *Deep-Sea Research Part I: Oceanographic Research Papers*, *92*, 93–106. <https://doi.org/10.1016/j.dsr.2014.06.011>
- Kim, T. W., Ha, H. K., Wählin, A. K., Lee, S. H., Kim, C. S., Lee, J. H., & Cho, Y. K. (2017). Is Ekman pumping responsible for the seasonal variation of warm circumpolar deep water in the Amundsen Sea? *Continental Shelf Research*, *132*, 38–48. <https://doi.org/10.1016/j.csr.2016.09.005>
- Kirby, R. R., & Beaugrand, G. (2009). Trophic amplification of climate warming. *Proceedings of the Royal Society B: Biological Sciences*, *276*(1676), 4095–4103. <https://doi.org/10.1098/rspb.2009.1320>
- Kistler, R., Kalnay, E., Collins, W., Saha, S., White, G., Woollen, J., et al. (2001). The NCEP-NCAR 50-year reanalysis: Monthly means CD-ROM and documentation. *Bulletin of the American Meteorological Society*, *82*(2), 247–267. [https://doi.org/10.1175/1520-0477\(2001\)082<0247:TNNYRM>2.3.CO;2](https://doi.org/10.1175/1520-0477(2001)082<0247:TNNYRM>2.3.CO;2)
- Liu, X., & Smith, W. O. (2012). Physiochemical controls on phytoplankton distributions in the Ross Sea, Antarctica. *Journal of Marine Systems*, *94*, 135–144. <https://doi.org/10.1016/j.jmarsys.2011.11.013>
- Mangoni, O., Saggiomo, V., Bolinesi, F., Margiotta, F., Budillon, G., Cotroneo, Y., et al. (2017). Phytoplankton blooms during austral summer in the Ross Sea, Antarctica: Driving factors and trophic implications. *PLoS ONE*, *12*(4), e0176033–e0176023. <https://doi.org/10.1371/journal.pone.0176033>
- Marchese, C., Albouy, C., Tremblay, J.-É., Dumont, D., D’Ortenzio, F., Vissault, S., & Bélanger, S. (2017). Changes in phytoplankton bloom phenology over the North Water (NOW) polynya: a response to changing environmental conditions. *Polar Biology*, *40*(9), 1721–1737. <https://doi.org/10.1007/s00300-017-2095-2>
- Markus, T. (1999). Results from an ECMWF-SSM/I forced mixed layer model of the Southern Ocean. *Journal of Geophysical Research-Oceans*, *104*(C7), 15603–15620. <https://doi.org/10.1029/1999JC900080>
- McGillicuddy, D. J., Sedwick, P. N., Dinniman, M. S., Arrigo, K. R., Bibby, T. S., Greenan, B. J. W., et al. (2015). Iron supply and demand in an Antarctic shelf ecosystem. *Geophysical Research Letters*, *42*, 8088–8097. <https://doi.org/10.1002/2015GL065727>

- Montes-Hugo, M. A., & Yuan, X. (2012). Climate patterns and phytoplankton dynamics in Antarctic latent heat polynyas. *Journal of Geophysical Research, Oceans*, *117*(C5). <https://doi.org/10.1029/2010JC006597>
- Mosby, A. F., & Smith, W. O. (2017). Structural equation modeling of the influence of environmental factors on summer phytoplankton growth in the Ross Sea. *Polar Biology*, *40*(2), 291–299. <https://doi.org/10.1007/s00300-016-1953-7>
- Murtaugh, P. A. (2009). Performance of several variable-selection methods applied to real ecological data. *Ecology Letters*, *12*(10), 1061–1068. <https://doi.org/10.1111/j.1461-0248.2009.01361.x>
- Myers, R. H. (1990). *Classical and modern regression with applications*. PWS-KENT (Second ed.). Boston: PWS-KENT. <https://doi.org/10.2307/1269347>
- Nelson, D. M., & Smith, W. O. (1991). Sverdrup revisited: Critical depths, maximum chlorophyll levels, and the control of Southern Ocean productivity by the irradiance-mixing regime. *Limnology and Oceanography*, *36*(8), 1650–1661. <https://doi.org/10.4319/lo.1991.36.8.1650>
- Nihashi, S., & Ohshima, K. I. (2015). Circumpolar mapping of antarctic coastal polynyas and landfast sea ice: Relationship and variability. *Journal of Climate*, *28*(9), 3650–3670. <https://doi.org/10.1175/JCLI-D-14-00369.1>
- Park, J., Kim, H. C., Jo, Y. H., Kidwell, A., & Hwang, J. (2018). Multi-temporal variation of the Ross Sea Polynya in response to climate forcings. *Polar Research*, *37*(1). <https://doi.org/10.1080/17518369.2018.1444891>
- Peloquin, J. A., & Smith, W. O. (2007). Phytoplankton blooms in the Ross Sea, Antarctica: Interannual variability in magnitude, temporal patterns, and composition. *Journal of Geophysical Research, Oceans*, *112*(C8), 1–12. <https://doi.org/10.1029/2006JC003816>
- Platt, T., & Sathyendranath, S. (2008). Ecological indicators for the pelagic zone of the ocean from remote sensing. *Remote Sensing of Environment*, *112*(8), 3426–3436. <https://doi.org/10.1016/j.rse.2007.10.016>
- Platt, T., White, G. N., Zhai, L., Sathyendranath, S., & Roy, S. (2009). The phenology of phytoplankton blooms: Ecosystem indicators from remote sensing. *Ecological Modelling*, *220*(21), 3057–3069. <https://doi.org/10.1016/j.ecolmodel.2008.11.022>
- Queste, B. Y., Heywood, K. J., Smith, W. O., Kaufman, D. E., Jickells, T. D., & Dinniman, M. S. (2015). Dissolved oxygen dynamics during a phytoplankton bloom in the Ross Sea polynya. *Antarctic Science*, *27*(4), 362–372. <https://doi.org/10.1017/S0954102014000881>
- Racault, M. F., Le Quéré, C., Buitenhuis, E., Sathyendranath, S., & Platt, T. (2012). Phytoplankton phenology in the global ocean. *Ecological Indicators*, *14*(1), 152–163. <https://doi.org/10.1016/j.ecolind.2011.07.010>
- Reddy, T. E., & Arrigo, K. R. (2006). Constraints on the extent of the Ross Sea phytoplankton bloom. *Journal of Geophysical Research, Oceans*, *111*(C7). <https://doi.org/10.1029/2005JC003339>
- Reddy, T. E., Arrigo, K. R., & Holland, D. M. (2007). The role of thermal and mechanical processes in the formation of the Ross Sea summer polynya. *Journal of Geophysical Research*, *112*(C7), C07027. <https://doi.org/10.1029/2006JC003874>
- Reynolds, R. W., Smith, T. M., Liu, C., Chelton, D. B., Casey, K. S., & Schlax, M. G. (2007). Daily high-resolution-blended analyses for sea surface temperature. *Journal of Climate*, *20*(22), 5473–5496. <https://doi.org/10.1175/2007JCLI1824.1>
- Rubao, J., Meibing, J., & Øystein, V. (2013). Sea ice phenology and timing of primary production pulses in the Arctic Ocean. *Global Change Biology*, *19*(3), 734–741. <https://doi.org/10.1111/gcb.12074>
- Ryan-Keogh, T. J., DeLizo, L. M., Smith, W. O., Sedwick, P. N., McGillicuddy, D. J., Moore, C. M., & Bibby, T. S. (2017). Temporal progression of photosynthetic-strategy in phytoplankton in the Ross Sea, Antarctica. *Journal of Marine Systems*, *166*, 87–96. <https://doi.org/10.1016/j.jmarsys.2016.08.014>
- Saba, V. S., Friedrichs, M. A. M., Antoine, D., Armstrong, R. A., Asanuma, I., Behrenfeld, M. J., et al. (2011). An evaluation of ocean color model estimates of marine primary productivity in coastal and pelagic regions across the globe. *Biogeosciences*, *8*(2), 489–503. <https://doi.org/10.5194/bg-8-489-2011>
- Salgado-Hernanz, P. M., Racault, M. F., Font-Muñoz, J. S., & Basterretxea, G. (2019). Trends in phytoplankton phenology in the Mediterranean Sea based on ocean-colour remote sensing. *Remote Sensing of Environment*, *221*(November 2018), 50–64. <https://doi.org/10.1016/j.rse.2018.10.036>
- Sapiano, M. R. P., Brown, C. W., Schollaert Uz, S., & Vargas, M. (2012). Establishing a global climatology of marine phytoplankton phenological characteristics. *Journal of Geophysical Research, Oceans*, *117*(C8), 1–16. <https://doi.org/10.1029/2012JC007958>
- Sasaoka, K., Chiba, S., & Saino, T. (2011). Climatic forcing and phytoplankton phenology over the subarctic North Pacific from 1998 to 2006, as observed from ocean color data. *Geophysical Research Letters*, *38*, L15609. <https://doi.org/10.1029/2011GL048299>
- Sedwick, P. N., & DiTullio, G. R. (1997). Regulation of algal blooms in Antarctic shelf waters by the release of iron from melting sea ice. *Geophysical Research Letters*, *24*(20), 2515–2518. <https://doi.org/10.1029/97GL02596>
- Sedwick, P. N., DiTullio, G. R., & Mackey, D. J. (2000). Iron and manganese in the Ross Sea, Antarctica: Seasonal iron limitation in Antarctic shelf waters. *Journal of Geophysical Research, Oceans*, *105*(C5), 11321–11336. <https://doi.org/10.1029/2000JC000256>
- Sedwick, P. N., Marsay, C. M., Sohst, B. M., Aguilar-Islas, A. M., Lohan, M. C., Long, M. C., et al. (2011). Early season depletion of dissolved iron in the Ross Sea polynya: Implications for iron dynamics on the Antarctic continental shelf. *Journal of Geophysical Research, Oceans*, *116*(C12), 1–19. <https://doi.org/10.1029/2010JC006553>
- Smith, W. O., Ainley, D. G., Arrigo, K. R., & Dinniman, M. S. (2014). The oceanography and ecology of the Ross Sea. *Annual Review of Marine Science*, *6*(1), 469–487. <https://doi.org/10.1146/annurev-marine-010213-135114>
- Smith, W. O., Asper, V., Tozzi, S., Liu, X., & Stammerjohn, S. E. (2011). Surface layer variability in the Ross Sea, Antarctica as assessed by in situ fluorescence measurements. *Progress in Oceanography*, *58*(1–4), 28–45. <https://doi.org/10.1016/j.pocean.2010.08.002>
- Smith, W. O., & Comiso, J. C. (2008). Influence of sea ice on primary production in the Southern Ocean: A satellite perspective. *Journal of Geophysical Research, Oceans*, *113*(C5), 1–19. <https://doi.org/10.1029/2007JC004251>
- Smith, W. O., Dennett, M. R., Mathot, S., & Caron, D. A. (2003). The temporal dynamics of the flagellated and colonial stages of *Phaeocystis* antarctica in the Ross Sea. *Deep-Sea Research Part II: Topical Studies in Oceanography*, *50*(3–4), 605–617. [https://doi.org/10.1016/S0967-0645\(02\)00586-6](https://doi.org/10.1016/S0967-0645(02)00586-6)
- Smith, W. O., Dinniman, M. S., Klinck, J. M., & Hofmann, E. (2003). Biogeochemical climatologies in the Ross Sea, Antarctica: Seasonal patterns of nutrients and biomass. *Deep-Sea Research Part II: Topical Studies in Oceanography*, *50*(22–26), 3083–3101. <https://doi.org/10.1016/j.dsr2.2003.07.010>
- Smith, W. O., Dinniman, M. S., Tozzi, S., DiTullio, G. R., Mangoni, O., Modigh, M., & Saggiomo, V. (2010). Phytoplankton photosynthetic pigments in the Ross Sea: Patterns and relationships among functional groups. *Journal of Marine Systems*, *82*(3), 177–185. <https://doi.org/10.1016/j.jmarsys.2010.04.014>
- Smith, W. O., & Gordon, L. I. (1997). Hyperproductivity of the Ross Sea (Antarctica) polynya during austral spring. *Geophysical Research Letters*, *24*(3), 233–236. <https://doi.org/10.1029/96GL03926>
- Smith, W. O., & Jones, R. M. (2015). Vertical mixing, critical depths, and phytoplankton growth in the Ross Sea. *ICES Journal of Marine Science*, *70*(4), 782–792. <https://doi.org/10.1093/icesjms/fst048>

- Smith, W. O., McGillicuddy, D. J., Olson, E. B., Kosnyrev, V., Peacock, E. E., & Sosik, H. M. (2017). Mesoscale variability in intact and ghost colonies of *Phaeocystis antarctica* in the Ross Sea: Distribution and abundance. *Journal of Marine Systems*, *166*, 97–107. <https://doi.org/10.1016/j.jmarsys.2016.05.007>
- Smith, W. O., Shields, A. R., Peloquin, J. A., Catalano, G., Tozzi, S., Dinniman, M. S., & Asper, V. A. (2006). Interannual variations in nutrients, net community production, and biogeochemical cycles in the Ross Sea. *Deep-Sea Research Part II: Topical Studies in Oceanography*, *53*(8–10), 815–833. <https://doi.org/10.1016/j.dsr2.2006.02.014>
- Smith, W. O., Tozzi, S., Long, M. C., Sedwick, P. N., Peloquin, J. A., Dunbar, R. B., et al. (2013). Spatial and temporal variations in variable fluorescence in the Ross Sea (Antarctica): Oceanographic correlates and bloom dynamics. *Deep-Sea Research Part I: Oceanographic Research Papers*, *79*, 141–155. <https://doi.org/10.1016/j.dsr.2013.05.002>
- Soppa, M. A., Völker, C., & Bracher, A. (2016). Diatom phenology in the Southern Ocean: Mean patterns, trends and the role of climate oscillations. *Remote Sensing*, *8*(5). <https://doi.org/10.3390/rs8050420>
- Taylor, A. H., Allen, J. I., & Clark, P. A. (2002). Extraction of a weak climatic signal by an ecosystem. *Nature*, *416*(6881), 629–632. <https://doi.org/10.1038/416629a>
- Toseland, A., Daines, S. J., Clark, J. R., Kirkham, A., Strauss, J., Uhlig, C., Lenton, T. M., et al. (2013). The impact of temperature on marine phytoplankton resource allocation and metabolism. *Nature Climate Change*, *3*(11), 979–984. <https://doi.org/10.1038/nclimate1989>
- Yamada, K., & Ishizaka, J. (2006). Estimation of interdecadal change of spring bloom timing, in the case of the Japan Sea. *Geophysical Research Letters*, *33*, L02608. <https://doi.org/10.1029/2005GL024792>
- Zhai, L., Platt, T., Tang, C., Sathyendranath, S., & Hernández Walls, R. (2011). Phytoplankton phenology on the Scotian Shelf. *ICES Journal of Marine Science*, *68*(4), 781–791. <https://doi.org/10.1093/icesjms/fsq175>
- Zwally, H. J., Comiso, J. C., & Gordon, A. L. (1985). Antarctic offshore leads and polynyas and oceanographic effects. *Oceanology of the Antarctic Continental Shelf*, 203–226. <https://doi.org/10.1029/AR043p0203>